Ab Initio Computational Studies of Mg Vacancy Diffusion in Doped MgB_2 Aimed at Hydriding Kinetics Enhancement of the $LiBH_4 + MgH_2$ System

Yang Zhong, Hong Zhu, Leon L. Shaw,* and R. Ramprasad

Department of Chemical, Materials and Biomolecular Engineering, University of Connecticut, Storrs, Connecticut 06269, United States

Received: July 17, 2010; Revised Manuscript Received: October 11, 2010

We report an ab initio density functional theory (DFT) study that investigates the effect of transition metal dopants on diffusion of Mg vacancies in MgB_2. This study has implications for the diffusion-controlled hydriding kinetics of the technologically important $LiBH_4 + MgH_2$ hydrogen storage system. The first-principles calculation reveals that the solubility of M (M = Ni, Mn, V, Ti, Sc, and Y) in MgB_2 and the migration barriers of Mg vacancies are dictated by the dopant's atomic radius, whereas the formation energies of Mg vacancies are strongly affected by both the dopant's atomic radius and charge distribution. Mn, Sc, and Y are found to have the potential to enhance the diffusion rate of Mg, whereas V and Ti are poor dopants in enhancing the diffusion rate of Mg in MgB_2. The findings in this study are consistent with existing experimental results.

1. Introduction

On-board hydrogen storage materials with high gravimetric and volumetric hydrogen densities have gained great interest as one of the key components for fuel-cell vehicles.[1] Lithium borohydride ($LiBH_4$), being one of the potential materials with the highest reversible hydrogen storage capacity (~18 wt %) for hydrogen vehicle applications, has been studied extensively.[1−4] However, bulk $LiBH_4$ can only be dehydrogenated and rehydrogenated above its melting temperature (~280 °C) because of its high chemical stability.[3−5] In fact, temperatures as high as 500 °C are required to release most of the hydrogen in $LiBH_4$.[4−19] One approach to reduce its dehydrogenation and rehydrogenation temperatures is to stabilize its dehydrogenated state by using additives,[6−13,20−25] as exemplified by the following equation:[6]

$$LiBH_4 + {}^1/_2MgH_2 = LiH + {}^1/_2MgB_2 + 2H_2 \qquad (1)$$

It is shown by Vajo et al.[6] that adding MgH_2 to $LiBH_4$ can lower the dehydrogenation enthalpy by ~25 kJ/mol H_2. In spite of the improvement in thermodynamic properties, the dehydrogenation and rehydrogenation temperatures for reaction 1 are still very high, near 350 °C.[6] Further studies[8−13]have revealed that hydrogen release does not proceed directly according to reaction 1, but with an intermediate reaction step. Because of the slow intermediate step, reaction 1 has only been destabilized thermodynamically, but not kinetically.[9]

To improve the reaction kinetics, catalysts such as $TiCl_3$, VCl_3, $NiCl_2$, and TiF_3 have been added to the $LiBH_4 + MgH_2$ system.[6,9,13] The addition of these catalysts has reduced the dehydrogenation temperatures by only 5 to 22 °C, indicating very limited effects of these catalysts and suggesting that diffusion in $LiBH_4$ and/or MgH_2 particles rather than interfacial reactions might be the rate-limiting step. To address the diffusion issue, effective ball milling of $LiBH_4 + MgH_2$ mixtures has been conducted recently at liquid nitrogen temperature with the addition of a small amount of graphite (5 vol %) to reduce the crystallite size of MgH_2 to ~60 nm and simultaneously convert crystalline $LiBH_4$ particles to amorphous.[26] The effectively ball milled $LiBH_4 + MgH_2$ mixture releases 4.0 wt % H_2 in the solid state at 265 °C, representing a 5-fold increase in the released hydrogen when compared with ineffectively ball milled counterparts. Indeed, releasing 4.0 wt % H_2 at 265 °C from the $LiBH_4 + MgH_2$ mixture is the best performance ever reported in the open literature. The typical values for releasing H_2 at the solid state reported by other studies[6,10,11,24] range from near zero to ~0.5 wt % H_2, depending on the processing and testing conditions.

Similar to dehydrogenation, the hydrogenation of reaction 1 also requires very stringent conditions, e.g., 400 °C and 100 bar hydrogen pressure.[6,11] However, it has been shown recently that solid-state hydriding at temperatures below 280 °C via reaction 1 is possible. Through long-time ball milling of LiH + MgB_2 mixtures, 8.3 wt % hydrogen uptake at 265 °C has been demonstrated.[27] This dramatic improvement in the hydriding property of the $LiBH_4 + MgH_2$ system over previous works[6,8,11] is attributed to the reduction of the particle and crystallite sizes of both LiH and MgB_2 to nanometers and the introduction of a large amount of structural defects to crystalline particles.[27] The phenomenological analysis of the hydriding kinetics unveils that both reduction in the particle and crystallite sizes and increase in the structural defects contribute to the enhancement in the diffusion-controlled hydriding reaction.[27] The detailed nuclear magnetic resonance (NMR) analysis[28−30] indicates that the diffusion-controlled hydrogenation is related to the formation of a ternary compound, $(Mg_{1-x}Li_{2x})B_2$ where x is a variable changing from 0 (for MgB_2) to less than 1, during hydrogenation. Diffusion arises because of the Li−Mg ion exchange to form the ternary diboride, $(Mg_{1-x}Li_{2x})B_2$, which facilitates the subsequent formation of $LiBH_4$ as hydrogenation proceeds.

The studies mentioned above[27−30] unequivocally show that further reduction in the hydriding temperature of the $LiBH_4 + MgH_2$ system can be achieved by (i) reducing particle sizes to minimize the diffusion distance, (ii) increasing diffusion coefficients via doping in MgB_2, and (iii) enhancing diffusion

* To whom correspondence should be addressed. E-mail: leon.shaw@uconn.edu.

10.1021/jp1066567
Published on Web 11/15/2010

coefficients through the introduction of a large number of defects to the crystalline MgB_2. In this context, a recent study[31] has revealed that the addition of the Mn dopant to the $LiH + MgB_2$ system can increase the hydriding kinetics, whereas the addition of the V dopant cannot. It has been postulated that the favorable effect of Mn is due to its strong capability to induce the lattice distortion of MgB_2 crystals and thus improve the diffusion rate of Mg.[31] The latter is essential for the formation of $LiBH_4$ from the ternary compound $(Mg_{1-x}Li_{2x})B_2$ during the hydriding reaction because complete removal of Mg from $(Mg_{1-x}Li_{2x})B_2$ by diffusion is needed for the formation of $LiBH_4$.

Here we report the first study using ab initio density functional theory (DFT) computations to investigate the effect of transition metal dopants on the diffusion of Mg vacancies in MgB_2. Such a study is inspired by the previous experimental work,[31] showing that the addition of the Mn dopant can improve the diffusion-controlled hydriding kinetics of the $LiH + MgB_2$ mixture. Given that Mg is the heaviest element in the ternary compound, $(Mg_{1-x}Li_{2x})B_2$, Mg is likely the slowest diffusing species. Thus, this investigation focuses on Mg diffusion in MgB_2. Ni, Mn, V, Ti, Sc, and Y have been selected for investigation because these dopants collectively allow the evaluation of the effects of the atomic radius of transition metals on Mg diffusion. In addition, to be effective dopants for enhancing Mg diffusion after multiple hydriding/dehydriding cycles, the doping element should possess some solubility in MgB_2. Since the solubilities of most transition metals in MgB_2 are not available in the open literature, the solubilities of transition metals in Mg[32] have been used as the criterion for selecting the aforementioned dopants. In this regard, Sc has the highest solubility in Mg (6 atom % at room temperature), followed by Y (1.5 atom %), Ti (0.12 atom %), and Mn (0.05 atom %), while V and Ni have essentially no solubility in Mg. Thus, selection of this group of transition metal dopants can provide a baseline for comparison of their solubilities in Mg and MgB_2. This first-principles study is expected to offer general guidelines in selecting proper transition metals as dopants to further enhance the diffusion of Mg and thus the hydriding kinetics of the $LiBH_4 + MgH_2$ system in the near future.

2. Calculation Method and Models

The DFT calculations were performed using the Vienna ab initio simulation package (VASP)[33,34] with the PW91 generalized gradient approximation (GGA),[35] projector-augmented wave (PAW) pseudopotentials, and a cutoff energy of 320 eV for the plane wave expansion of the wave functions. MgB_2 consists of interleaved graphite-like layers of B atoms and triangular layers of Mg.[36,37] As most transition metals form an isostructural compound MB_2 with boron, like AlB_2, CrB_2, MnB_2, etc.,[38] we have used a $3 \times 3 \times 3$ supercell of MgB_2 containing a total of 27 Mg and 54 B atoms (Figure 1), and replaced one Mg atom with M (M = Ni, Mn, V, Ti, Sc, or Y) to investigate the dopant's impact on the tendency for Mg vacancy formation and migration. A $2 \times 2 \times 2$ Monkhorst−Pack k-point mesh has been used to attain converged results for these supercell calculations.

The magnesium boride solid solution, $Mg_{1-x}M_xB_2$, can be regarded as the product of the following reaction:

$$MgB_2 + xM = Mg_{1-x}M_xB_2 + xMg \qquad (2)$$

The formation energy of the solid solution is defined as $\Delta E = E_{Mg_{1-x}M_xB_2} + xE_{Mg} - xE_M - E_{MgB_2}$, where $E_{Mg_{1-x}M_xB_2}$ and E_{MgB_2} represent the DFT energies of MgB_2 with and without dopants, while E_{Mg} and E_M are the energies for one Mg atom and one M atom in their elemental states, respectively.

The Mg vacancy formation energy, E_f, is defined as $E_f = E_{vac} + E_{Mg} - E_{perf}$, where E_{vac} and E_{perf} are the DFT energies for the system with and without Mg vacancy and E_{Mg} is the energy for one Mg atom in its elemental state. The energy barriers for the Mg diffusion are calculated by using the nudged elastic band method.[39] Both out-of-plane and in-plane diffusions are considered for the migration of Mg vacancies. Due to the close-packed structure of the Mg plane, the Mg vacancy will migrate to the closest Mg atom site for the in-plane diffusion, such as from A to B site (path 2) or from A to A site (path 3) in Figure 1a. For the out-of-plane diffusion the Mg vacancy will diffuse through the center of the boron hexagon of its graphene-like structure to the Mg atom site in the next Mg plane, as shown in Figure 1c.

It should be mentioned that the accuracy of the prediction based on the state-of-the-art DFT calculations is high. As discussed in a recent work,[40] DFT calculations have been used to predict many properties of materials, such as geometry, bulk modulus, work function, barrier energy, etc., with high accuracy. For the present study, the calculated lattice parameters are 3.07 Å for a and 3.52 Å for c, in good agreement with the experimental values at 37 K (3.08 Å for a and 3.51 Å for c).[41] On the basis of these numbers, the difference between calculated and measured lattice parameters is less than 0.5%.

3. Results and Discussion

3.1. Formation Energies of Boride Solid Solutions. Figure 2 shows the formation energies of magnesium boride solid solutions, $Mg_{1-x}M_xB_2$, as a function of the atomic radius for various M. Note that the formation energies for all the doping elements except Ni are negative, suggesting that all of the elements except Ni are favorable to be doped into MgB_2. Furthermore, the formation energy is a strong function of the atomic radius[42] of the doping element. The elements with atomic radii close to that of Mg have much favorable energies for forming boride solid solutions. This finding is in good accordance with Hume−Rothery's rule of 15% size difference for forming metallic solid solutions with good solubility.[43] It is noted that our prediction about the solubility of the six transition elements is consistent with available experimental reports about the successful synthesis of magnesium boride solid solutions, $Mg_{1-x}M_xB_2$ (where M = Mn, Ti, and Sc), using multiple methods.[39,44−48]

3.2. Formation Energies of Mg Vacancies. As shown in Figure 1, there are five different Mg vacancy sites in the $3 \times 3 \times 3$ supercell with respect to the position of the doping element M. In the AB plane (the M-containing plane in Figure 1a) there are only two types of Mg atomic sites, i.e., types A and B, which are the first and second neighboring Mg positions to the dopant M. In the CDE plane (the M-free plane in Figure 1b) there are three types of Mg atomic sites, i.e., types C, D, and E. The Mg site just above or below M is site C, and sites D and E are the first and second neighboring Mg atoms to site C.

The formation energy of Mg vacancies (E_f) for pure MgB_2 is calculated to be 2.26 eV, whereas the formation energies of Mg vacancies at different sites (A, B, C, D and E) as a function of dopant's radius are summarized in Figure 3. On the basis of a simplified view of stresses caused by dopants, one may expect the following trend in vacancy formation energies. A dopant atom smaller (larger) than Mg results in local tensile (compressive) stresses which will disfavor (favor) the formation of vacancies as they will tend to further increase the respective

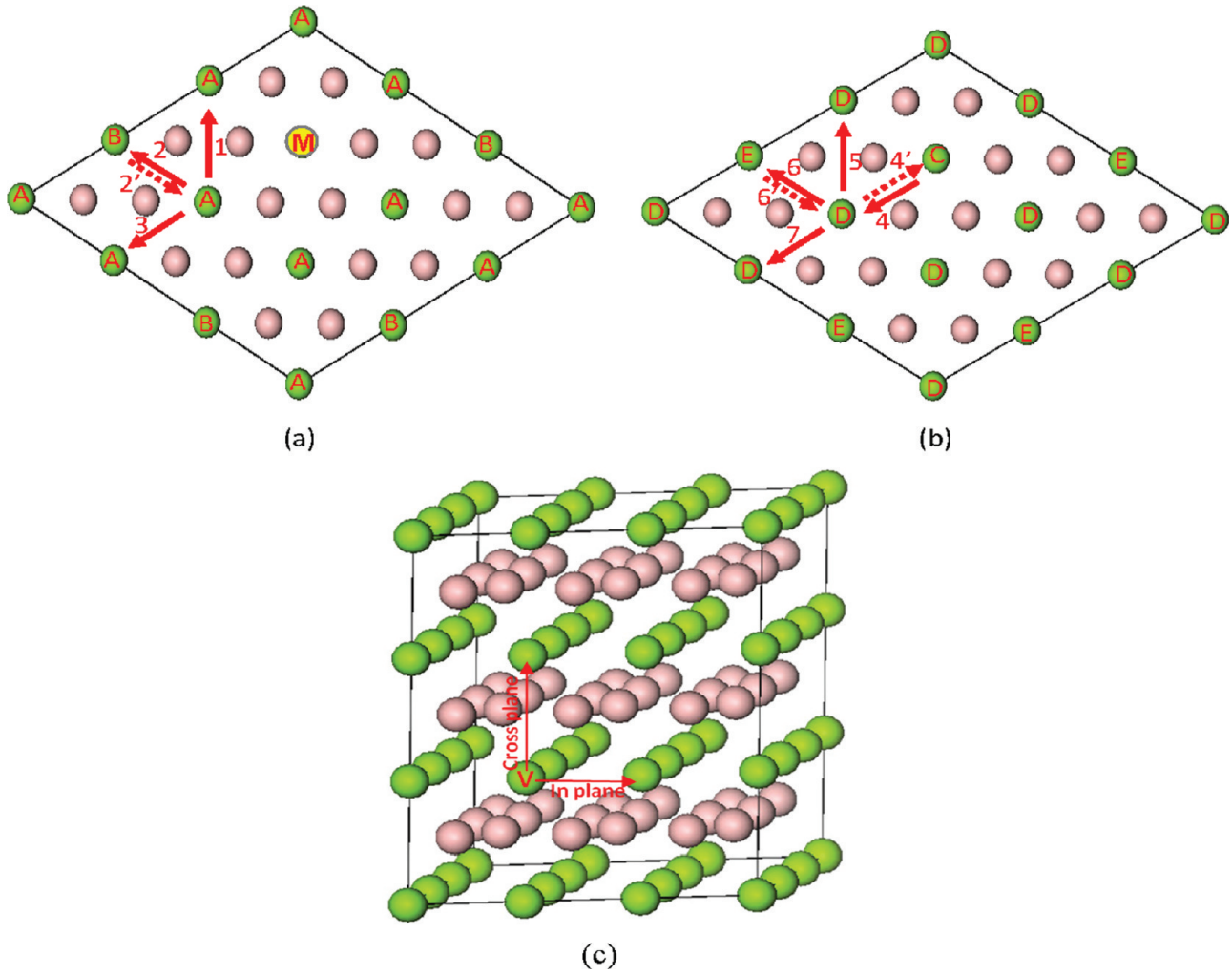

Figure 1. The MgB_2 supercell with Mg and B atoms shown as green and pink spheres respectively: (a) the top view of a Mg plane containing Mg atoms, A and B, with a doping atom at the site labeled with M (termed the AB plane hereafter), (b) the top view of the Mg plane adjacent to the AB plane showing the positions of Mg atoms, C, D, and E (called the CDE plane), and (c) the side view of the MgB_2 supercell with one Mg vacancy created at the site labeled with V. The positions of boron atoms are shown in all of these figures. The Mg atoms, A to E, in parts a and b are due to the nonequivalent Mg vacancy sites with respect to the doping atom, M. The possible diffusion paths for these nonequivalent Mg vacancies are shown as red arrows and labeled with numbers.

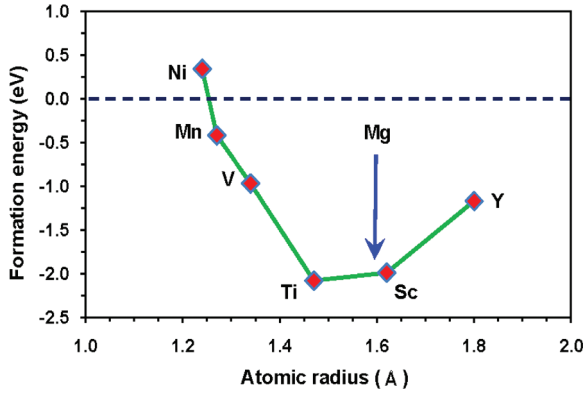

Figure 2. The formation energies of magnesium boride solid solutions, $Mg_xM_{1-x}B_2$, as a function of the atomic radius of the doping element, M. The atomic radius of Mg is 1.6 Å as indicated by the arrow.

stresses. In other words, one may expect a smaller dopant atom to lead to larger vacancy formation energies. From Figure 3, it can be seen that this trend is followed only in systems containing dopants smaller than Mg (barring for the C type vacancy which lies directly below the dopant atom with an intervening M atom). In general, the vacancy formation energy is larger in the presence of dopants (regardless of size) than in the case of pure MgH_2. For example, V, Ti, and Sc (the last two with their atomic radii close to that of Mg) offer the smallest increase in the formation energy of Mg vacancy, while the other dopants result in much larger increases. This implies that factors other than atomic size

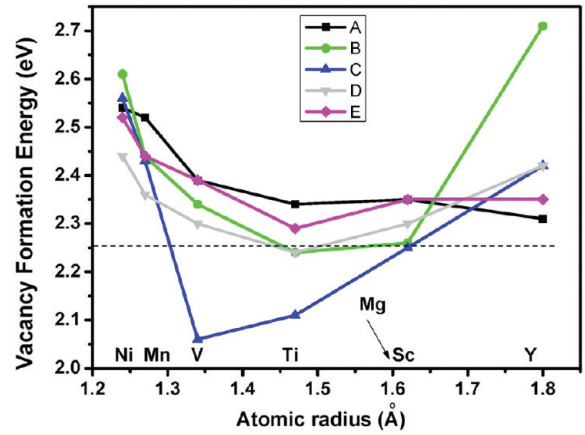

Figure 3. The formation energy of Mg vacancy at different sites (A, B, C, D, and E) as a function of the dopant's atomic radius. The dashed line stands for E_f in pure MgB_2. See Figure 1 for the locations of A−E sites.

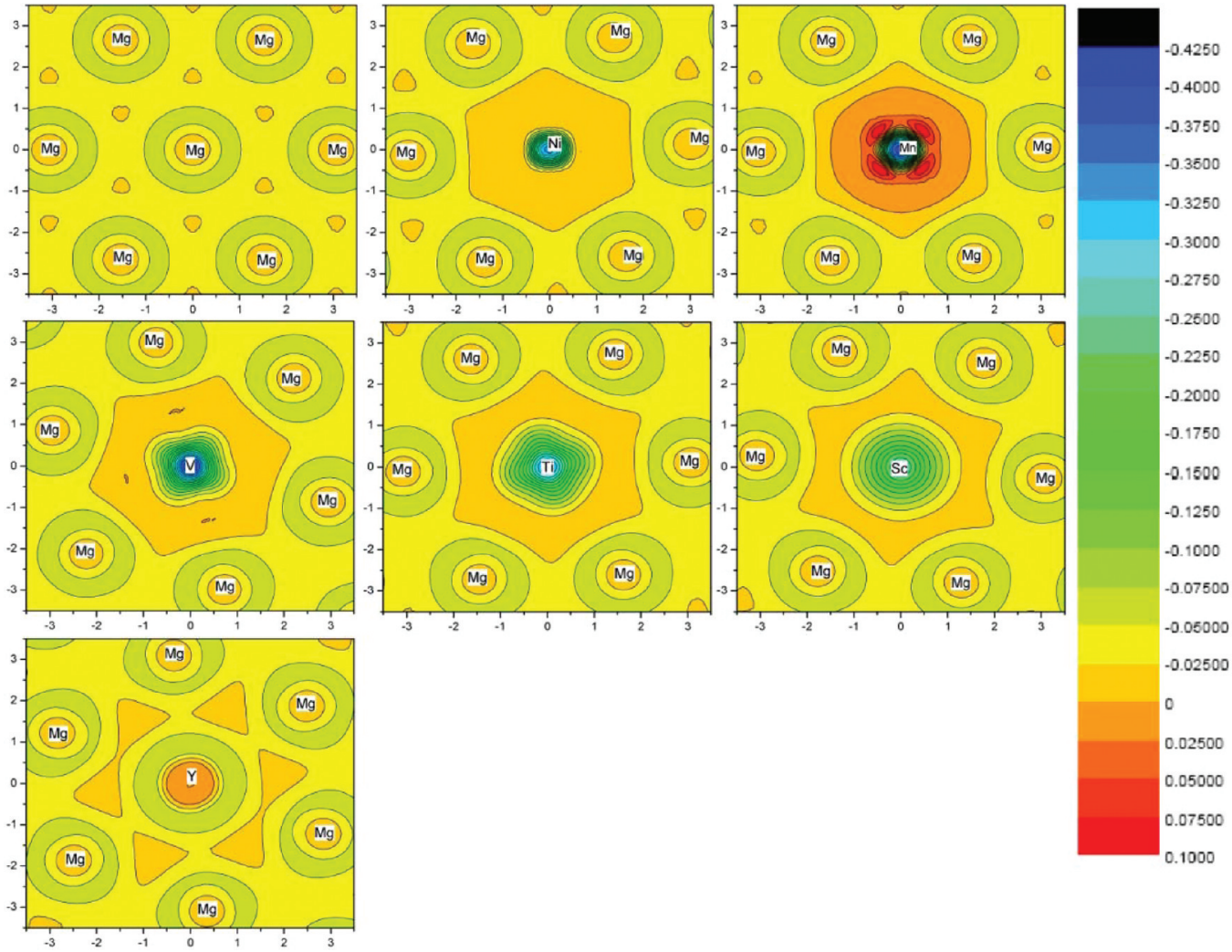

Figure 4. The difference charge densities of $Mg_xM_{1-x}B_2$ within the AB plane (i.e., the M-containing plane). Negative/positive charge densities indicate charge depletion/accumulation. The distance is given in Å.

(e.g., electronegativity or electron affinity of the atoms, or ionicity of the bonds) must play a role in determining the tendency for vacancy formation.

To understand the possible effect of the charge distribution of the dopant on the different behaviors shown in Figure 3, we plot in Figure 4 the charge density difference between the solid and atoms within the AB plane. The planar charge density maps for Ni- and Mn-doped MgB_2 are similar, that is, the charge depletes within a small region around Ni and Mn atoms. For V-, Ti-, and Sc-doped MgB_2, they behave similarly, having a larger depleted region, while Y-doped MgB_2 has a similar charge distribution as pure MgB_2. Thus, the charge distribution within the AB plane displays the same similarities and differences among the six transition elements as the trend of the vacancy formation energy shown in Figure 3, suggesting that the formation energies for Mg vacancies are strongly affected by the charge distribution of the dopant. Overall, the higher formation energies for Mg vacancies in $Mg_{1-x}M_xB_2$ than that in MgB_2 suggest the necessity of pre-existing Mg vacancies in order to improve the hydrogenation kinetics of $Mg_{1-x}M_xB_2$, which can be achieved via high-energy ball milling.[27]

3.3. Migration Barriers of Mg Vacancies. The calculated energy barrier for the in-plane migration of Mg vacancies in pure MgB_2 (1.80 eV) is much smaller than that for the out-of-plane diffusion (4.87 eV). The result clearly reveals that the Mg vacancy will tend to diffuse in-plane rather than out-of-plane. Thus, in what follows we will focus on the effect of the transition metal dopants on the in-plane diffusion. The in-plane migration of Mg vacancies in $Mg_xM_{1-x}B_2$ has been considered for both AB and CDE planes (Figure 1a,b). For completeness, we have studied all the possible in-plane migration paths in the $3 \times 3 \times 3$ supercell. The possible diffusion paths are 1, 2, or 3 in the AB plane and 4, 5, 6, or 7 in the CDE plane. We note that for diffusion paths 2, 4, and 6, the starting and ending sites are not equivalent; thus the migrations along the opposite directions (2′, 4′, and 6′) are also considered.

Figure 5 shows the energy profiles along various diffusion paths in the AB plane for different doping elements. The results unveil that Ni, Y, and Sc doping can decrease the Mg vacancy migration barriers along some paths, while the other doping elements either have no effect or increase the migration barriers. For example, Ni doping decreases the migration barrier along path 1 from 1.8 to 1.4 eV, while Y doping decreases the migration barriers along paths 2, 2′, and 3 from 1.8 eV to 1.65, 1.65, and 1.69 eV, respectively.

Again, we attempt to correlate the trends in the migration barriers with the dopant size. Note that in addition to the atomic size of the dopant, other factors such as electronegativity, ionicity, etc. are bound to play a role. However, the latter factors are expected to drop off faster than the atomic size factor away from the dopant. Thus, barriers for migration paths farther from the dopant will be mainly controlled by the dopant atomic size.

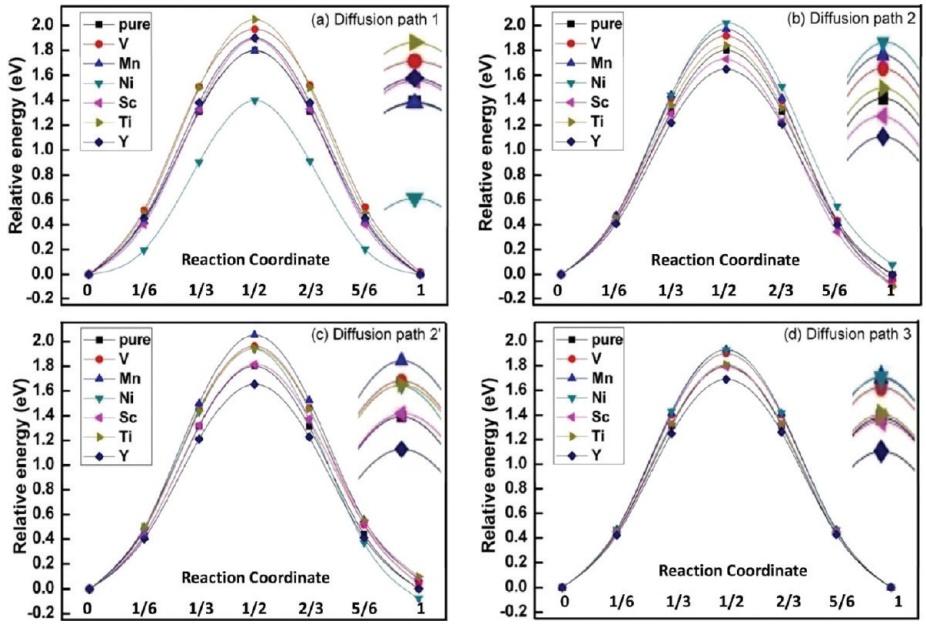

Figure 5. Calculated relative energies of Mg diffusion in the AB plane along paths (a) 1, (b) 2, (c) 2′, and (d) 3. For clarity, the enlarged view of peaks is shown on the right of each figure.

We also expect that dopants with sizes similar to that of Mg will have similar barriers. These expectations are borne out in the migration barrier results when the results shown in Figure 5 are replotted in Figure 6a as a function of the atomic radius of the dopant. For instance, migration barriers for paths 2, 2′, and 3 (Figure 6a) show a clear and strong dependence on atomic size. The barriers for Ti and Sc dopants (those with sizes closest to Mg) display barriers most similar to that in the undoped case. Barriers for path 1 do not follow the same trend. This is presumably because this pathway is closest to the dopant atom, and is hence influenced by the other factors mentioned above.

We note that a Mg vacancy (at either site A or B) can diffuse from one side to the other side of the 3 × 3 × 3 supercell through a combination of paths 2, 2′, and 3 in the AB plane (Figure 1a). The combined path will be called a complete path in this study, whereas paths 2, 2′, and 3 that form the complete path will be termed subpaths hereafter. It should be emphasized that the presence of complete paths is necessary for Mg vacancies to diffuse within the entire MgB_2 crystal under composition gradients. It is well-known that the diffusion coefficient, D, is proportional to $\exp(-E_m/kT)$, where E_m is the migration barrier for diffusion. Thus, whether a Mg vacancy can diffuse quickly from one side of the 3 × 3 × 3 supercell to the other side depends on the presence of low migration barriers for all the subpaths that form a complete path. If the migration barrier for one of the subpaths is very high, then diffusion of the Mg vacancy along this complete path will be severely limited because diffusion of the Mg vacancy along this subpath will be very slow and becomes the rate-limiting step. Thus, the simultaneous reduction in the migration barriers along the subpaths 2, 2′, and 3 that form a complete path is essential and can greatly enhance the diffusion rate of Mg. In this regard, Y and Sc are effective dopants because they decrease the migration barriers along subpaths 2, 2′, and 3 (Figure 6a). In contrast, V and Ti are poor dopants because they increase the migration barriers for all subpaths (Figure 6a). However, Ni and Mn may or may not be helpful because they decrease the migration barrier along subpath 1 while increasing the migration barriers along the other subpaths. Subpath 1 alone is not sufficient to allow a Mg vacancy to diffuse from one side to the other side of the supercell, and thus the effect of Ni and Mn on Mg diffusion in the AB plane cannot be clearly defined from Figure 6a.

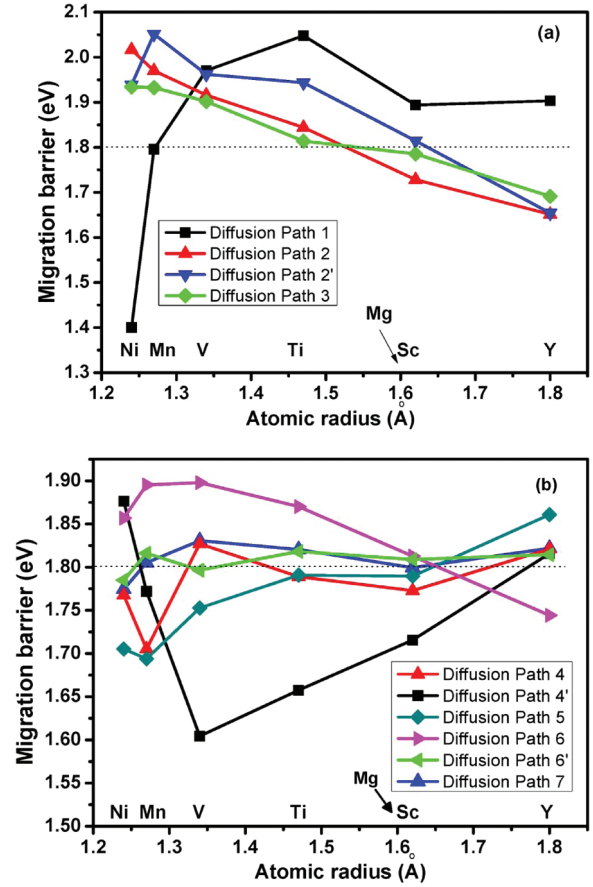

Figure 6. The migration barriers along different paths as a function of the dopant's atomic radius (a) showing diffusion paths 1, 2, 2′, and 3 in the AB plane and (b) showing diffusion paths 4, 4′, 5, 6, 6′, and 7 in the CDE plane. The migration barrier for all paths in the undoped MgB_2 is 1.8 eV as shown by the horizontal dashed line.

The migration barriers for Mg vacancies in the CDE plane along all the possible diffusion subpaths (4, 4′, 5, 6, 6′, and 7)

are shown in Figure 6b. Compared to the dopant-containing AB plane, the dopant's impact on Mg vacancy migration in the CDE plane is smaller. The biggest impact on migration barriers is seen in subpath 4′, a path that includes the C type vacancy site. Dopants with atomic radius close to the Mg radius of 1.6 Å have the smallest effect on migration barriers. Interestingly, every dopant can reduce the migration barriers along some subpaths. However, a detailed examination reveals that V, Ti, and Y are poor dopants because they do not offer complete paths with low migration barriers to permit a Mg vacancy at either site E or D to diffuse from one side of the supercell to the other side (Figure 1b). In contrast, Ni, Mn, and Sc are effective dopants because they provide complete paths with low migration barriers for a Mg vacancy at site D to diffuse from one side of the supercell to the other side. For example, a Mg vacancy at site D in the CDE plane of a Sc- or Mn-doped MgB_2 can diffuse along subpaths 7, 4′, and 4 with low migration barriers from one side of the supercell to site D at the other side of the supercell. Similarly, a Mg vacancy at site D in the CDE plane of a Ni-doped MgB_2 can diffuse along subpaths 7, 5, 5, and 5 with low migration barriers from one side to the other side of the supercell.

Thus, considering the results of the AB and CDE planes together, we conclude that V and Ti are poor dopants, whereas Mn, Sc, and Y are good dopants with the potential to enhance the diffusion rate of Mg in MgB_2 and thus to increase the hydriding kinetics of the $LiH + MgB_2$ system. In the case of Ni, although it has the potential to enhance the diffusion rate of Mg in MgB_2 as discussed above, it does not make a good solid solution with MgB_2 due to its high formation energy (Figure 2). The conclusion reached by this first-principles calculation is in good agreement with the previous experimental study,[31] showing that the V dopant does not enhance the hydriding kinetics of the $LiH + MgB_2$ system even though V is dissolved in MgB_2. In contrast, the Mn dopant exhibits a favorable effect in enhancing the hydriding kinetics of the $LiH + MgB_2$ system because Mn induces more lattice distortion of MgB_2 crystals than V does.[31] It should also be stressed that the conclusion reached from this study is only applicable to the hydriding process of the $LiBH_4 + MgH_2$ system because the dehydriding process of the $LiBH_4 + MgH_2$ system is unlikely to be controlled by the diffusion of Mg in MgB_2. This argument is supported by the fact that the reactants are $LiBH_4$ and MgH_2 while the product of MgB_2 may or may not form in the dehydriding process of the $LiBH_4 + MgH_2$ system.[8−12,26] This is the reason why Mn doping enhances the hydriding kinetics but not the dehydriding kinetics, whereas V doping exhibits no effect on the hydriding kinetics but enhances the dehydriding kinetics, as observed in experiments.[31]

Finally, it should be pointed out that the addition of Ti via titanium trichloride[6] or titanium isopropoxide[13] to the $LiH + MgB_2$ system has been shown to enhance the kinetics of hydrogenation. However, those experiments[6,13] are conducted at the liquid state (i.e., at temperatures above the melting point of $LiBH_4$). With the presence of liquid, the rate-limiting step for hydrogenation may change from the solid-state diffusion to the interfacial reaction such as the hydrogen adsorption on the surface of the liquid. Under this condition, the Ti derived from titanium trichloride or titanium isopropoxide may act as a catalyst to enhance the interfacial reaction, and thus exhibits favorable effects in improving the hydrogenation kinetics.[6,13] However, the Ti dopant has little effect on enhancing the diffusion rate of Mg in MgB_2 at the solid state, as predicted in this study. It is anticipated that additional work is needed in the future to clearly define the exact role of Ti in improving the hydrogenation kinetics at the liquid state.

4. Concluding Remarks

The present study offers the first investigation using ab initio DFT computations to explore the possibility of enhancing diffusion of Mg vacancies in MgB_2 with transition metal dopants and thus improving the diffusion-controlled hydriding kinetics of the $LiBH_4 + MgH_2$ system. The major conclusions drawn from this study are as follows:

(1) The formation energy of the magnesium boride solid solution is mainly determined by the dopant's atomic radius. Dopants with atomic radii close to that of Mg have favorable energies for the formation of magnesium boride solid solutions.

(2) The formation energy of the Mg vacancy is affected by both the atomic radius and charge distribution of the dopant. In general, dopants with atomic radii close to that of Mg lead to smaller increases in the formation energy of the Mg vacancy.

(3) The migration barrier of Mg vacancies is strongly controlled by the dopant's atomic radius unless the migration path is close to the dopant. When the migration path in a dopant-containing plane is not close to the dopant, the migration barrier decreases with increasing the dopant size. In contrast, the migration barrier may increase, decrease, or change little with increasing the dopant size on the dopant-free plane, depending on the specific migration path.

(4) Dopants with the capability to offer low migration barriers for complete pathways that connect one end of the supercell to another will enhance diffusion of Mg vacancies in MgB_2. On the basis of this criterion, Mn, Sc, and Y dopants have been identified to have the potential to enhance the diffusion rate of Mg in MgB_2 and thus the hydriding kinetics of the $LiH + MgB_2$ system, whereas V and Ti dopants do not. The predicted trend matches the available experimental result of Mn and V dopants well.

(5) On the basis of the criterion of low migration barriers for complete pathways that connect one end of the supercell to another, one can conclude that dopants with a large difference in their atomic sizes from that of Mg have the potential to enhance the diffusion rate of Mg in MgB_2. The only exception to this general rule is Sc, which has an atomic radius similar to that of Mg.

There are several implications when applying the conclusions above to other transition metal dopants that have not been investigated in this study. Dopants with a large difference in their atomic sizes from that of Mg have the potential to enhance the diffusion rate of Mg in MgB_2 and thus enhance the hydrogenation kinetics of the $LiH + MgB_2$ system at the solid state. However, a large difference in the atomic size from that of Mg is unfavorable for forming magnesium boride solid solutions. The Ni dopant falls into this category. Therefore, in selecting dopants to enhance the hydrogenation kinetics the effects of the dopants on the formation energies of boride solid solutions and the migration barriers of Mg vacancies should be considered simultaneously. The formation energy of Mg vacancies is another important factor in selecting dopants. The present study reveals that the charge distribution of the dopant plays an important role in the formation energy of Mg vacancies. However, more detailed studies are needed in the future to relate the charge distribution to the electron affinity of the atoms and/or ionicity of the bonds so that the judgment on the formation energy of Mg vacancies can be made through factors that are more readily available than the charge distribution of the dopant.

Acknowledgment. The research was sponsored by the U.S. Department of Energy (DOE) under contract no. DE-FC36-05GO15008 with Dr. Ned T. Stetson as the Technology Manager.

References and Notes

(1) Schlapbach, L.; Zuttel, A. *Nature* **2001**, *414*, 353–358.
(2) Soulie, J.; Renaudin, G.; Cerny, R.; Yvon, K. *J. Alloys Compd.* **2002**, *346*, 200–205.
(3) Zuttel, A.; Wenger, P.; Rentsch, S.; Sudan, P.; Mauron, Ph.; Emmenegger, Ch. *J. Power Sources* **2003**, *118*, 1–7.
(4) Orimo, S.; Nakamori, Y.; Kitahara, G.; Miwa, K.; Ohba, N.; Towata, S.; Zuttel, A. *J. Alloys Compd.* **2005**, *404−406*, 427–430.
(5) Zuttel, A.; Rentsch, S.; Fischer, P.; Wenger, P.; Sudan, P.; Mauron, Ph.; Emmenegger, Ch. *J. Alloys Compd.* **2003**, *356−357*, 515–520.
(6) Vajo, J. J.; Skeith, S. L.; Mertens, F. *J. Phys. Chem. B* **2005**, *109*, 3719–3722.
(7) Meisner, G. P.; Scullin, M. L.; Balogh, M. P.; Pinkerton, F. E.; Meyer, M. S. *J. Phys. Chem. B* **2006**, *110*, 4186–4192.
(8) Yu, X. B.; Grant, D. M.; Walker, G. S. *Chem. Commun.* **2006**, 3906–3908.
(9) Vajo, J. J.; Salguero, T. T.; Gross, A. F.; Skeith, S. L.; Olson, G. L. *J. Alloys Compd.* **2007**, *446−447*, 409–414.
(10) Nakagawa, T.; Ichikawa, T.; Hanada, N.; Kojima, Y.; Fujii, H. *J. Alloys Compd.* **2007**, *446−447*, 306–309.
(11) Pinkerton, F. E.; Meyer, M. S.; Meisner, G. P.; Balogh, M. P.; Vajo, J. J. *J. Phys. Chem. C* **2007**, *111*, 12881–12885.
(12) Walker, G. S.; Grant, D. M.; Price, T. C.; Yu, X. B.; Legrand, V. *J. Power Sources* **2009**, *194*, 1128–1134.
(13) Bösenberg, U.; Doppiu, S.; Mosegaard, L.; Barkhordarian, G.; Eigen, N.; Borgschulte, A.; Jensen, T. R.; Cerenius, Y.; Gutfleisch, O.; Klassen, T.; Dornheim, M.; Bormann, R. *Acta Mater.* **2007**, *55*, 3951–3958.
(14) Kostka, J.; Lohstroh, W.; Fichtner, M.; Hahn, H. *J. Phys. Chem. C* **2007**, *111*, 14026–14029.
(15) Vajo, J. J.; Olson, G. L. *Scr. Mater.* **2007**, *56*, 829–834.
(16) Gross, A. F.; Vajo, J. J.; Van Atta, S. L.; Olson, G. L. *J. Phys. Chem. C* **2008**, *112*, 5651–5657.
(17) Yu, X. B.; Wu, Z.; Chen, Q. R.; Li, Z. L.; Weng, B. C.; Huang, T. S. *Appl. Phys. Lett.* **2007**, *90*, 034106.
(18) Zhang, Y.; Zhang, W.-S.; Wang, A.-Q.; Sun, L.-X.; Fan, M.-Q.; Chu, H.-L.; Sun, J.-C.; Zhang, T. *Int. J. Hydrogen Energy* **2007**, *32*, 3976–3980.
(19) Zuttel, A.; Borgschulte, A.; Orimo, S.-i. *Scr. Mater.* **2007**, *56*, 823–828.
(20) Vajo, J. J.; Skeith, S. L.; Mertens, F.; Jorgensen, S. W. *J. Alloys Compd.* **2005**, *390*, 55–61.
(21) Nakamori, Y.; Ninomiya, A.; Kitahara, G.; Aoki, M.; Noritake, T.; Miwa, K.; Kojima, Y.; Orimo, S.-i. *J. Power Sources* **2006**, *155*, 447–455.
(22) Au, M.; Jurgensen, A. *J. Phys. Chem. B* **2006**, *110*, 7062–7067.
(23) Au, M.; Jurgensen, A.; Zeigler, K. *J. Phys. Chem. B* **2006**, *110*, 26482–26487.
(24) Yang, J.; Sudik, A.; Wolverton, C. *J. Phys. Chem. C* **2007**, *111*, 19134–19140.
(25) Siegel, D. J.; Wolverton, C.; Ozolins, V. *Phys. Rev. B* **2007**, *76*, 134102.
(26) Crosby, K.; Shaw, L. *Int. J. Hydrogen Energy* **2010**, *35*, 7519–7529.
(27) Wan, X.; Markmaitree, T.; Osborn, W.; Shaw, L. *J. Phys. Chem. C* **2008**, *112*, 18232–18243.
(28) Hu, J. Z.; Kwak, J. H.; Yang, Z. G.; Wan, X.; Shaw, L. *Appl. Phys. Lett.* **2009**, *94*, 141905.
(29) Hu, J. Z.; Kwak, J. H.; Yang, Z. G.; Wan, X.; Shaw, L. *J. Power Sources* **2010**, *195*, 3645–3648.
(30) Shaw, L.; Wan, X.; Hu, J. Z.; Kwak, J. H.; Yang, Z. G. *J. Phys. Chem. C* **2010**, *114*, 8089–8098.
(31) Crosby, K.; Wan, X.; Shaw, L. *J. Power Sources* **2010**, *195*, 7380–7385.
(32) Massalski, T. B.; Murray, J. L.; Bennett, L. H.; Baker, H., Eds. *Binary Alloy Phase Diagrams*; ASM International: Materials Park, OH, 1986.
(33) Kresse, G.; Hafner, J. *Phys. Rev. B* **1993**, *47*, 558–561.
(34) Kresse, G.; Furthmuller, J. *Phys. Rev. B* **1996**, *54*, 11169–11186.
(35) Perdew, J. P.; Chevary, J. A.; Vosko, S. H.; Jackson, K. A.; Pederson, M. R.; Singh, D. J.; Fiolhais, C. *Phys. Rev. B* **1992**, *46*, 6671–6687.
(36) Barkhordarian, G.; Jensen, T. R.; Doppiu, S.; Bsenberg, U.; Borgschulte, A.; Gremaud, R.; Cerenius, Y.; Dornheim, M.; Klassen, T.; Bormann, R. *J. Phys. Chem. C* **2008**, *112*, 2743–2749.
(37) Jemmis, E. D.; Jayasree, E. G. *Acc. Chem. Res.* **2003**, *36*, 816–824.
(38) Xu, S.; Moritomo, Y.; Kato, H.; Nakamura, A. *J. Phys. Soc. Jpn.* **2001**, *70*, 1889–1891.
(39) Henkelman, G.; Johnson, H. *J. Chem. Phys.* **2000**, *113*, 9978.
(40) Ramprasad, R.; Shi, N.; Tang, C. Modeling the Physics and Chemistry of Interfaces in Nanodielectrics. In *Dielectric Polymer Nanocomposites*, Nelson, J. K., Ed.; Springer: New York, 2010.
(41) Jorgensen, J. D.; Hinks, D. G.; Short, S. *Phys. Rev. B* **2001**, *63*, 224522.
(42) Greenwood, N. N.; Earnshaw, A. *Chemistry of the Elements*, 2nd ed.; Butterworth-Heinemann: Oxford, UK, 1997.
(43) Haasen, P. *Physical Metallurgy*, 3rd ed.; Cambridge University Press: Cambridge, UK, 1996; p 140.
(44) Xu, S.; Moritomo, Y.; Nakamura, A. *J. Phys. Soc. Jpn.* **2002**, *71*, 326–328 (Supplement).
(45) Prikhna, T. A.; Gawalek, W.; Savchuk, Y. M.; Moshchil, V. E.; Sergienko, N. V.; Habisreuther, T.; Wendt, M.; Hergt, R.; Schmidt, Ch.; Dellith, J.; Melnikov, V. S.; Assmann, A.; Litzkendorf, D.; Nagorny, P. A. *Physica C* **2004**, *402*, 223–233.
(46) Goto, D.; Machi, T.; Zhao, Y.; Koshizuka, N.; Murakami, M.; Arai, S. *Physica C* **2003**, *392−396*, 272–275.
(47) Agrestini, S.; Metallo, C.; Filippi, M.; Campi, G.; Sanipoli, C.; De Negri, S.; Giovannini, M.; Saccone, A.; Latini, A.; Bianconi, A. *J. Phys. Chem. Solids* **2004**, *65*, 1479–1484.
(48) Agrestini, S.; Metallo, C.; Filippi, M.; Simonelli, L.; Campi, G.; Sanipoli, C. *Phys. Rev. B* **2004**, *70*, 134514.

JP1066567